Development of a textural characterization index for mineral liberation studies based on grain morphology and particle-scale relationships

Percy Escalante[1], Josep Oliva[1], Hernán Anticoi[1] and Carlos Hoffmann Sampaio[1]

[1] Departament d'Enginyeria Minera, Industrial i TIC (EMIT), Universitat Politècnica de Catalunya - BarcelonaTech (UPC), Av. Bases de Manresa 61-73, 08242 Manresa, Spain

Abstract

Quantitative characterization of mineral textures is essential for understanding mineral liberation and optimizing mineral processing performance. This study proposes a novel Texture Index (TI) derived from Mineral Liberation Analyzer (MLA) data, integrating geometric and topological relationships between mineral grains and their host particles. The index combines three dimensionless factors describing grain shape, grain-border complexity and mineral surface occupancy within particles. A scaling factor constrains the TI to a maximum value of 3, representing volume conservation under ideal textural conditions. The proposed methodology enables a quantitative assessment of texture that incorporates both individual grain morphology and collective grain arrangements. To evaluate its behaviour and interpretability, the TI factors are compared with conventional shape descriptors, including circularity, aspect ratio and grain angularity. Results demonstrate that the index captures textural attributes not fully represented by traditional morphological parameters, providing a complementary metric for mineral liberation and textural characterization in process mineralogy.

1 Introduction

Mineral texture is a multiscale characteristic that describes how mineral phases are geometrically and spatially organized within a rock or particle. It encompasses mineral composition, grain size and size distribution, grain shape and orientation, grain-boundary irregularity, mineral associations and the spatial arrangement of grains, including structures such as inclusions, veins, bands and clusters (Ferrara et al., 1989; Hilden and Powell, 2017; Månbro et al., 2025). Consequently, texture cannot be represented adequately by mineral composition or grain size alone, because particles with similar mineral contents may exhibit markedly different internal arrangements and processing responses.

Accurate mineral-texture identification is essential for liberation studies because comminution behaviour depends not only on the grain-to-particle size ratio, but also on grain shape, boundary characteristics, intergrowths and mineral distribution. Grain size indicates the grinding fineness required, whereas grain boundaries and intergrowth patterns influence whether breakage occurs along mineral contacts or within mineral phases (Pérez-Barnuevo et al., 2013; Månbro et al., 2025). Consequently, ores with similar mineralogy and grain size may exhibit different liberation responses because of contrasting textures. These textural differences also affect subsequent separation processes, such as flotation. Pérez-Barnuevo et al. (2012, 2013) highlighted that composition-based liberation may differ from liberation based on exposed mineral surface, potentially overestimating recovery. Particle characterization should therefore combine mineral proportion with exposed surface, phase contacts, intergrown boundaries and boundary complexity, particularly in ores with complex intergrowths.

Several approaches have attempted to express texture quantitatively through an index or coefficient (Ersoy and Waller, 1995; Ueda et al., 2017; Atici and Comakli, 2019; Voigt et al., 2019; Karakaya et al. 2025; Ardalanzdeh et al., 2026). An early example was the textural rank proposed by Ferrara et al. (1989), which related mineral-inclusion geometry to liberation behaviour in simplified two-phase textures. The proposed textural rank ranges from 1 for platy or banded textures to 3 for granular or blocky textures, with rod-like and intermediate geometries occupying values between these limits. The study suggests that this parameter can help predict mineral liberation, particularly when particle size approaches the characteristic inclusion size.

A parallel development in rock engineering was the texture coefficient, originally introduced as a dimensionless parameter that combines several geometrical and structural characteristics of intact rock into a single quantitative value. The parameters incorporated into this coefficient include grain circularity or form factor, the number and aspect ratio of elongated grains, their orientation and the relative proportion of grains and matrix represented by packing density (Ersoy and Waller, 1995; Ozturk and Nasuf, 2013). Subsequent studies expanded this framework by incorporating additional descriptors, including grain area, perimeter, axial dimensions, equivalent diameter, compactness, interlocking and textural homogeneity (Mikaeil et al., 2022; Karakaya et al., 2025). These methods were applied to diverse sedimentary, igneous, metamorphic and carbonate rocks, primarily to predict strength, drillability, cuttability and related engineering properties (Ozturk et al., 2014; Atici and Comakli, 2019; Kamani and Ajalloeian, 2019). Although these coefficients were not developed specifically for mineral liberation, they demonstrated the value of integrating multiple textural descriptors into a single quantitative measure.

At the particle scale, Pérez-Barnuevo et al. (2012, 2013) developed and applied textural indices integrating mineral proportion, exposed perimeter, phase contacts and intergrown boundaries. Their texture complexity index compares the real intergrown surface with the minimum theoretical surface, distinguishing simple from complex intergrowths and reflecting grain-boundary irregularity. Following studies expanded this approach through statistical and three-dimensional (3D) methods. Ueda et al. (2017) evaluated texture indices for correcting stereological bias in liberation measurements, while Hilden and Powell (2017) developed a geometrical multi-mineral model and Voigt et al. (2019) combined X-ray computed tomography with 3D statistical descriptors to characterize drill-core textures. These developments improved the representation of mineral arrangement across particle and rock scales. These advances are particularly relevant to Mineral Liberation Analyzer (MLA), Quantitative Evaluation of Minerals by Scanning Electron Microscopy (QEMSCAN) and related scanning electron microscopy coupled with energy-dispersive X-ray spectroscopy (SEM–EDS) platforms, which provide detailed particle-level data from polished two-dimensional (2D) sections but remain subject to stereological bias when estimating the true 3D liberation state (Fandrich et al., 2007; Leißner et al., 2016).

Despite these advances, no standardized framework currently exists for quantifying ore texture in mineral-processing applications. Existing methods are generally designed for specific purposes and often describe only selected textural attributes. A key remaining challenge is to translate quantitative rock-texture information into meaningful descriptors of particle populations and mineral liberation (Månbro et al., 2025). In this context, the present study develops a particle-based texture index from MLA data. The proposed index integrates three complementary attributes: the morphology of individual mineral grains, the cumulative complexity of their boundaries within the particle and the proportion of the target mineral

occupying the host particle. Each factor ranges from 0 to 1, while a scaling factor constrains the index to a maximum value of 3 under ideal textural conditions. This upper limit is conceptually supported by the 3D nature of mineral particles: under conservation of mineral and gangue phase volumes, the volume of geometrically similar particles varies with the cube of their characteristic size (King, 2001). The response of index is evaluated against conventional morphological descriptors, including circularity, aspect ratio and angularity, and against particle-scale variables such as grain size, particle size and the number of grains per particle. The proposed framework is intended to complement conventional liberation measurements by providing a single quantitative and interpretable metric that combines individual grain morphology with collective grain–particle relationships.

2 Material and methods

2.1 Material

The sample used in this study is a quartz-rich sand with a particle size below 2 mm, collected from the municipality of Bellpuig in the province of Lleida, Catalonia, Spain. Geologically, the material belongs to Quaternary detrital deposits of predominantly alluvial origin, formed through the accumulation of sediments transported by ancient fluvial systems during the Pleistocene (Mata, 2012).

2.2 Analytical methods

MLA was used for the mineralogical characterization of the material and to obtain textural parameters associated with the measurable geometry of grains and particles (area, perimeter and diameter). A total of nine samples representing different size fractions were analysed (Table 1). The samples were mounted in resin and prepared as 30 mm-diameter polished sections. Measurements were conducted at the SEM–MLA laboratory of Memorial University of Newfoundland, Canada, using a FEI MLA 650FEG system.

Table 1. Analysed samples and their particle-size ranges

Sample	Particle Size (µm)
BP1	+10-500
BP2	+60-1400
BP3	+10-1000
BP4	+20-355
BP5	+10-180
BP6	+20-2000
BP7	+20-1000
BP8	+10-710
BP9	+10-500

As described by Gu (2003) and Fandrich et al. (2007), MLA combines backscattered-electron (BSE) imaging with EDS to identify and classify mineral phases. These authors also indicate that the system incorporates an automated deagglomeration function to reduce the effects of

particles that are touching or agglomerated during analysis. BSE images distinguish mineral particles from the resin based on grayscale contrast, whereas EDS analysis provides information on the elemental composition of the phases present. However, during the preparation of resin-mounted samples, some particles may remain joined or in contact, potentially introducing errors into particle-size, shape and liberation measurements. To minimize this effect, automated deagglomeration uses shape parameters, edge detection, linear-feature recognition, and erosion and dilation procedures. SEM–MLA measurements are performed on polished sections; therefore, the results provide a 2D representation of 3D particles and grains. In this study, size, shape and textural parameters were interpreted directly from the areas, perimeters and geometrical relationships measured in the analysed sections. Consequently, the results may be affected by stereological bias (Leißner et al., 2016) and should be regarded as a 2D representation of mineral texture, without the application of subsequent stereological or 3D corrections.

2.3 Texture Index (TI)

The calculation of the TI is based on a geometrical interpretation of particles and their constituent grains, assuming a circular approximation of their shapes. For this purpose, each particle is treated in this study as a binary mineral-of-interest–gangue system. Under this approach, a mineral of interest is selected and the textural factors describing its occurrence within the particle are calculated, while all remaining mineral phases are grouped into a single complementary phase representing the gangue. This simplification allows multicomponent particles to be represented as binary systems, thereby facilitating the geometrical assessment of texture and its relationship with mineral liberation. Similar approaches have been applied in studies of mineral-liberation prediction for binary systems, such as those developed by Zhang and Subasinghe (2013) and Lee et al. (2022).

The index is calculated as the product of three dimensionless factors and a constant, defined using fundamental geometrical parameters such as perimeter and area obtained from the MLA results. These parameters make it possible to quantify grain morphology and the spatial relationship between the grains and the particles that contain them. Based on these criteria, the TI is defined for each particle by the following expression:

$$TI = F_f \cdot B_f \cdot S_f \cdot 3 \quad (1)$$

where F_f is a form factor describing the morphology of the grains contained within the particle; B_f represents the relationship between grain perimeters; S_f represents the ratio between the total grain area and the total particle area; and 3 is a constant associated with volumetric conservation between the mineral phase and the particle.

The TI has a maximum value of 3, in accordance with the phase-volume conservation criterion. Consequently, each of its component factors has a maximum value of 1. Andrews and Mika (1975) introduced this principle to define the attainable grade limits of particles generated by fracture. King (2001) subsequently incorporated the effect of mineral texture and established that the exponent associated with these geometrical relationships cannot exceed 3, because particle volume scales with the cube of a characteristic length. Values greater than 3 would therefore imply exceeding the volume of the mineral phase available in the original particle, which would not be physically consistent. Within this framework, the maximum TI is attained

when the particle consists of a single circular grain, representing the ideal condition of a fully liberated particle.

A circular geometry provides a clear reference for normalizing F_f and B_f because, for a given area, a circle has the minimum perimeter. Thus, a single circular grain allows both factors to reach 1, whereas elongation, angularity, boundary irregularity or subdivision reduce their values. This common maximum also facilitates their integration with S_f, which likewise reaches 1 when the mineral of interest occupies the entire particle. The multiplicative formulation of the TI allows F_f, B_f and S_f to be integrated as simultaneous conditions of mineral texture. Unlike an arithmetic mean, in which high values may offset low ones, multiplication penalizes a decrease in any individual factor. This is relevant because a favourable texture requires, at the same time, morphologically regular grains, a compact geometrical arrangement and a substantial proportion of the mineral of interest within the particle. Therefore, the product of the factors provides a more restrictive representation of the interaction among grain shape, geometrical arrangement and mineral proportion.

2.3.1 Form Factor (F_f)

This factor is calculated for each particle as the median ratio between the circular-equivalent perimeter of each grain and its actual perimeter, considering all grains contained within the particle. It is expressed as:

$$F_f = \text{median}_{i=1}^{n}\left(2\sqrt{\pi Ag_i}/Pg_i \right) \quad (2)$$

where Ag_i is the area of grain i, Pg_i is the actual perimeter of grain i, and n is the total number of grains within the particle. These data are obtained directly from the MLA results.

F_f measures the regularity or roundness of the grains within a particle through a perimeter ratio calculated individually for each grain. Therefore, this factor evaluates the intrinsic morphology of each grain before the information is integrated using the median. Its values range from 0 to 1, with higher values indicating more symmetrical grains that are closer to a circular shape, whereas lower values reflect more irregular morphologies.

The median is used because it provides a more robust representation of the central tendency of individual grain morphology and reduces the influence of extreme values associated with highly irregular grains or strongly contrasting grain sizes. This prevents a small number of atypical grains from dominating the final factor value.

2.3.2 Boundary Factor (B_f)

B_f represents the ratio between the perimeter of a circle with an area equivalent to the sum of the areas of all grains and the sum of the actual perimeters of those grains within a particle. This factor evaluates the overall geometric compactness or irregularity of the grain assemblage. It is also calculated for each particle and is expressed as:

$$B_f = 2\sqrt{\pi \sum_{i=1}^{n} Ag_i}/\sum_{i=1}^{n} Pg_i \quad (3)$$

This factor provides an integrated interpretation of the grains because it does not evaluate each grain separately, but rather the geometrical behaviour of the assemblage as a whole. B_f compares an ideal circular geometry, constructed from the total area occupied by the grains,

with their actual cumulative perimeter. Its values range from 0 to 1, with higher values indicating a more compact grain assemblage with lower overall irregularity, whereas lower values reflect greater angularity or boundary complexity.

The main difference from F_f is that F_f describes the individual regularity of the grains, whereas B_f summarizes the overall geometrical expression of the grain assemblage within the particle. Therefore, B_f indicates whether the mineral of interest occurs as a more compact domain or as multiple grains with a larger cumulative perimeter, while also reflecting greater angularity or irregularity of the grain boundaries.

2.3.3 Surface Factor (S_f)

S_f represents the ratio between the total area occupied by the grains of the mineral of interest and the total area of the particle containing them. This factor expresses the proportion of the mineral within the particle through an area ratio and can therefore be interpreted as a 2D approximation of mineral grade derived from the MLA results. For each particle, it is expressed as:

$$S_f = \left(\sum_{i=1}^{n} Ag_i\right)/Ap \quad (4)$$

where Ap is the total area of the particle.

S_f values range from 0 to 1. Values close to 1 indicate that the mineral of interest occupies a large proportion of the particle area and therefore exhibits a higher degree of liberation. In contrast, low values reflect a lower mineral proportion and greater association with other phases. Unlike F_f and B_f, which describe the individual or collective morphology of the grains, S_f directly incorporates the relationship between the grains and the entire particle. It therefore represents the proportion of space occupied by the mineral phase within the particle, consistently with the volume-conservation criterion as interpreted in 2D.

2.4 Grain shape characterization

Three shape parameters obtained from MLA measurements were used to characterize grain morphology: circularity, aspect ratio and angularity (Table 2). These parameters were previously described for particle analysis by Escalante et al. (2025, 2026), who detailed their definitions and application to the interpretation of particulate-material behaviour. In this study, these parameters were adapted to the analysis of mineral grains and related to the TI.

Table 2. Definition of shape parameters obtained from MLA (Escalante et al. 2026).

Shape Parameter	Definition
Circularity	$4\pi A / P^2$; where A = Area and P = Perimeter of the particle.
Aspect ratio	B / L; where B = Breadth and L = Length of a minimum bounding rectangle of the particle.
Angularity	Σ ((Radius) − (Radius Equivalent Ellipse)) / (Radius Equivalent Ellipse]) in 1° increments of the particle.

Circularity measures how closely the outline of a grain resembles a circular shape, based on the relationship between its area and perimeter. Its maximum value is 1 and decreases as the boundary becomes more irregular or concave. Aspect ratio describes the degree of grain elongation from the relationship between its width and length. Values close to 1 indicate more equidimensional grains, whereas lower values reflect more elongated shapes. Angularity quantifies grain-boundary irregularity associated with the presence of corners, sharp edges or protrusions. Low values indicate more rounded shapes, whereas high values reflect more angular and irregular grains.

3 Results and discussion

3.1 Material mineralogical composition

Modal mineralogy obtained by MLA indicates that the samples are dominated by quartz and carbonates, with feldspars and phyllosilicates occurring as secondary phases (Table 3). Quartz is the principal mineral in all samples, generally accounting for approximately half or more of the total mass. Calcite is the second most abundant phase, although its proportion varies among samples. Among the silicates, orthoclase, plagioclase and muscovite are the main associated minerals. Dolomite, chlorite and tourmaline occur in lower proportions, generally at low concentrations but recurrently across the analysed samples. Taken together, this mineral assemblage is consistent with the detrital and alluvial nature of the material.

Table 3. MLA modal mineralogy by sample.

Mineral	Wt%								
	BP1	**BP2**	**BP3**	**BP4**	**BP5**	**BP6**	**BP7**	**BP8**	**BP9**
Quartz	49.44	67.73	75.88	51.55	39.80	72.68	69.42	58.57	45.49
Calcite	20.40	21.37	8.50	17.92	27.38	12.72	10.58	13.31	21.87
Orthoclase	11.64	4.87	9.54	12.06	6.59	6.44	10.90	15.04	12.30
Plagioclase	7.22	2.31	3.42	7.77	7.15	5.03	6.60	8.83	10.16
Muscovite	6.61	2.68	1.88	6.74	6.32	1.71	0.80	1.66	2.54
Dolomite	2.54	0.01	0.02	1.91	8.18	0.50	0.45	0.97	4.18
Chlorite	0.69	0.69	0.38	0.71	0.95	0.34	0.30	0.44	0.68
Tourmaline	0.58	0.28	0.20	0.73	0.98	0.39	0.43	0.58	1.23
Iron Oxide	0.29	0.01	0.05	0.28	0.92	0.05	0.04	0.04	0.33
Biotite	0.16	0.02	0.08	0.12	0.23	0.02	0.01	0.04	0.13
Rutile	0.13	0.01	0.02	0.08	0.46	0.01	0.01	0.01	0.10
Apatite	0.06	0.01	0.02	0.05	0.16	0.02	0.18	0.03	0.06
Pyroxene	0.06	-	0.01	0.01	0.08	0.03	0.07	0.14	0.29
Hornblende	0.03	-	-	0.01	0.04	0.03	0.18	0.14	0.23
Ilmenite	0.01	-	0.01	0.02	0.20	0.01	-	-	0.04
Staurolite	0.13	-	-	0.02	0.23	0.01	-	0.03	0.26
Zircon	0.02	-	-	0.01	0.30	0.01	0.01	-	0.03
Titanite	-	-	-	0.02	0.02	0.01	0.01	0.16	0.05
Monazite	-	-	-	-	-	-	-	-	0.02
Barite	-	0.01	-	-	-	-	-	-	-

3.2 Target mineral for TI calculation

In this study, tourmaline was used as the reference mineral for calculating the textural parameters. This phase was selected because it was consistently identified and quantified by MLA in all analysed samples, at concentrations ranging from 0.20 to 1.23 wt%. In addition, the dataset includes 7,961 tourmaline-bearing particles and 34,460 tourmaline grains (Table 4), providing a sufficiently robust quantitative basis to evaluate its textural variability as a first approximation in the application of the index.

Table 4. Number of tourmaline-bearing particles and tourmaline grains per sample.

No.	Sample									Total
	BP1	BP2	BP3	BP4	BP5	BP6	BP7	BP8	BP9	
Particles	1,366	24	68	1,436	2,887	158	220	463	1,339	7,961
Grains	5,284	672	1,257	7,868	7,378	2,500	2,152	3,053	4,296	34,460

Although tourmaline is an accessory phase, it exhibits sufficient morphological variability to evaluate the response of the Texture Index. Its occurrence ranges from small disseminated grains associated with low-grade particles and showing a relatively symmetrical morphology to fully liberated particles dominated by tourmaline. Between these extremes, intermediate occurrences include elongated grains and more massive domains with angular boundaries within multicomponent particles (Fig. 1). This variability enables a more comprehensive assessment of the relationships among mineral grade, mode of occurrence and grain morphology.

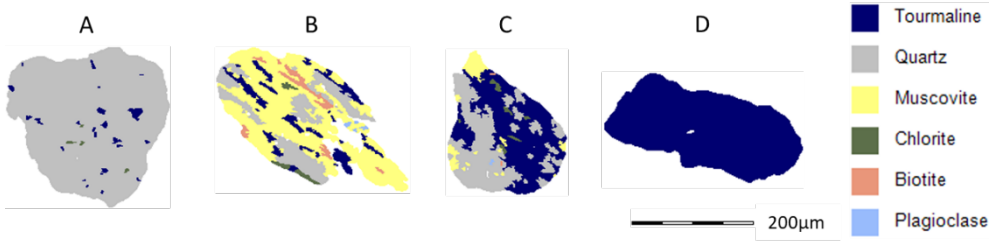

Figure 1. Representative occurrences of tourmaline grains. (A) disseminated grains, (B) elongated grains, (C) angular domain and (D) fully liberated particle.

3.3 Effect of grain and particle size on textural factors

3.3.1 Textural factors as a function of grain size

Fig. 2 shows the variation in F_f, B_f, and S_f across the different grain-size classes. F_f remained relatively constant, with most values concentrated between approximately 0.5 and 0.8 and no clear systematic trend with increasing grain size. This indicates that grain morphology, in terms of roundness and shape regularity, was largely independent of grain size. The finest classes showed comparatively lower variability, whereas a broader dispersion was observed in some intermediate and coarse classes, reflecting greater morphological heterogeneity.

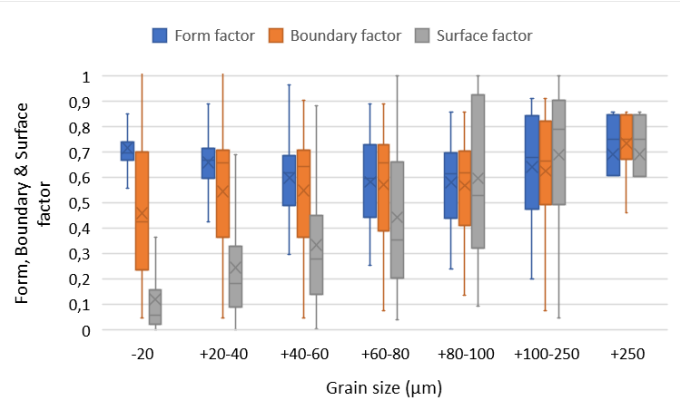

Figure 2. Textural factors by grain size.

In contrast, B_f exhibited a slight increase with grain size, although considerable overlap occurred between adjacent classes. Lower B_f values in the finer fractions are consistent with a more fragmented mineral distribution, potentially involving a larger number of grains and therefore a greater cumulative grain perimeter relative to the mineral area. Conversely, the higher B_f values observed in the coarser fractions suggest a more compact mineral distribution, with fewer or larger mineral domains and a lower relative perimeter.

S_f showed the clearest relationship with grain size, increasing progressively from the finest to the coarsest classes. Fine grains were mainly associated with particles containing a low proportion of the target mineral, whereas coarse grains tended to occupy a larger fraction of the particle area. Therefore, increasing grain size was associated with higher particle grade and a greater degree of mineral exposure or liberation. Overall, the results indicate that grain size has a limited influence on grain shape but a stronger effect on mineral distribution and mineral proportion within the particles.

3.3.2 Textural factors as a function of particle size

Particle size showed contrasting effects on the three textural factors. F_f remained relatively stable across all size classes, with most values concentrated between approximately 0.6 and 0.8. The limited variation in the median values indicates that grain roundness and morphological regularity were largely independent of particle size. As shown in Fig. 3, no systematic change in grain shape was observed as particle size increased.

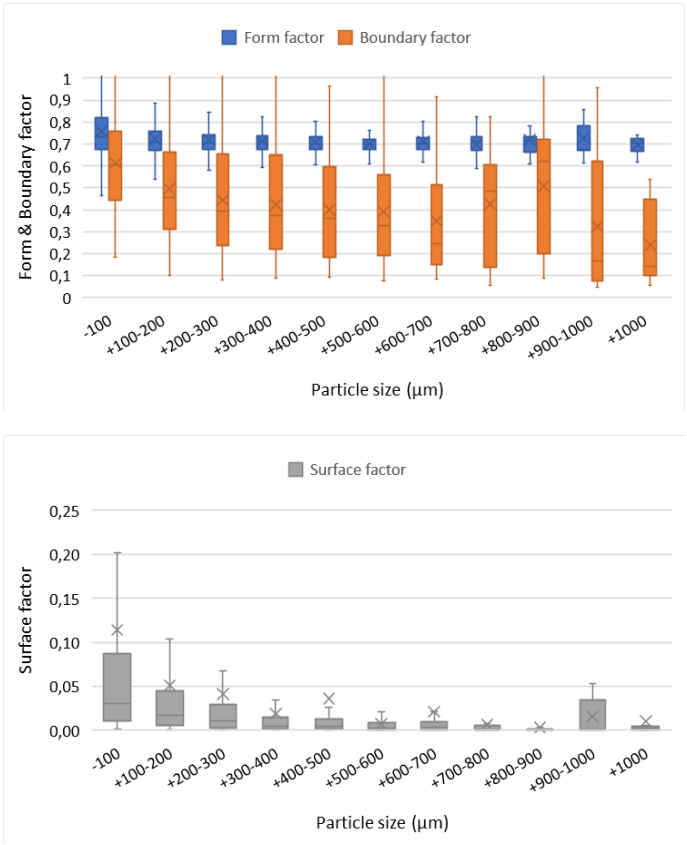

Figure 3. Textural factors by particle size.

In contrast, B_f displayed a broad distribution, with most values ranging from approximately 0.1 to 0.7, and an overall tendency to decrease with increasing particle size. This behaviour suggests that larger particles have a greater probability of containing multiple mineral grains. The resulting increase in cumulative grain perimeter relative to the total mineral area produces lower B_f values. Although local variability was observed among some coarse size classes, the general trend indicates a more dispersed and internally complex mineral distribution within larger particles.

S_f was predominantly concentrated between 0 and 0.2 and exhibited an inverse relationship with particle size. The finest particles showed the highest values and greatest variability, whereas S_f approached zero in most coarse size classes. This indicates that finer particles generally contained a higher proportion of the target mineral and therefore exhibited a greater degree of liberation. Conversely, the low S_f values recorded for larger particles reflect a lower mineral proportion and stronger association with gangue. Overall, particle size had little influence on grain shape but exerted a clearer control on mineral distribution and liberation, with increasing particle size generally associated with lower B_f and S_f values.

3.4 Effect of mineral proportion and grain population on the TI

3.4.1 TI as a function of S_f

The texture index increased consistently with S_f, showing a strong positive relationship between mineral proportion within the particle and textural quality. As shown in Fig. 4, particles with S_f below 0.1 displayed texture index values close to zero, whereas progressively higher values were observed as S_f increased. The texture index exceeded approximately 0.8 for S_f values between 0.8 and 0.9 and reached its maximum average value, approximately 1.7, in the 0.9–1.0 interval.

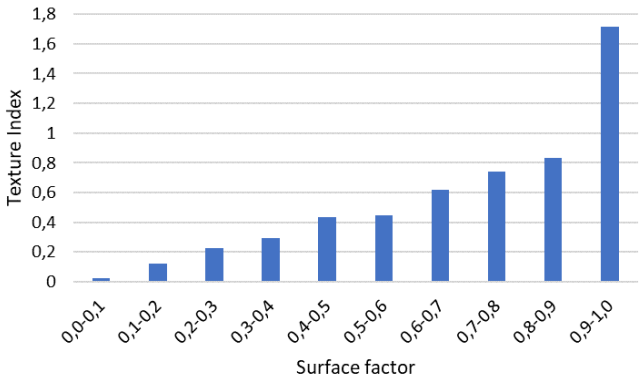

Figure 4. Variation of the TI with mineral proportion (S_f).

This behaviour is consistent with the multiplicative contribution of S_f to the texture index. Particles containing a low proportion of the target mineral are strongly penalised, even when their grain morphology and boundary characteristics are favourable, even when their grain morphology and boundary characteristics are favourable. Conversely, particles with high S_f values contain a greater proportion of the target mineral and are generally associated with higher liberation, resulting in a marked increase in the texture index. The particularly pronounced increase in the highest S_f interval indicates that particles approaching monomineralic composition attain substantially higher textural index values. Overall, S_f appears to be the most influential factor controlling the texture index, highlighting particle mineral content and liberation as the dominant textural characteristics captured by the index.

3.4.2 TI as a function of grains per particle

The texture index showed a clear negative relationship with the number of mineral grains contained within each particle. Particles composed of a single grain exhibited the highest texture index, followed by a marked decrease in particles containing between one and five grains. The index continued to decline as the number of grains increased, reaching values close to zero in particles containing more than 40 grains, as shown in Fig. 5.

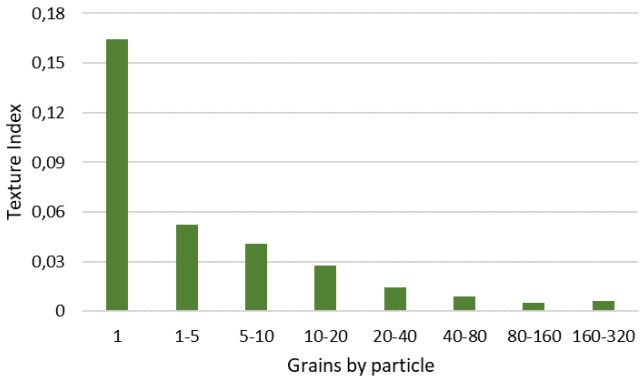

Figure 5. Variation of the TI with the number of grains per particle.

This behaviour reflects the influence of mineral distribution and particle grade on the texture index. Particles containing fewer grains are more likely to comprise large and compact mineral domains that occupy a greater proportion of the particle area, resulting in higher S_f and B_f values. In contrast, an increasing number of grains produces a greater cumulative grain perimeter and generally reflects a more finely disseminated mineral distribution. These characteristics reduce both B_f and, particularly, S_f, thereby decreasing the texture index.

Taken together, the results indicate that high texture index values are predominantly associated with particles containing few mineral grains and a high proportion of the target mineral. Conversely, particles containing numerous grains tend to be more compositionally complex, less liberated and characterised by lower texture index values. Thus, although the number of grains is not included directly in the texture index equation, it exerts an important indirect influence through its relationship with mineral grade, grain-boundary complexity and liberation.

The particle examples presented in Fig. 6 further illustrate this relationship. Although the selected particles have comparable sizes and similar tourmaline contents, represented by comparable S_f values, the target mineral occurs with different degrees of subdivision. The particle containing a single, relatively compact tourmaline grain exhibits the highest texture index, whereas the index progressively decreases when the same mineral proportion is distributed among several smaller grains. Increasing the number of grains increases the cumulative mineral perimeter and therefore reduces B_f, even when particle size and grade remain relatively constant. This comparison confirms that the texture index is sensitive not only to the mineral proportion within the particle but also to the internal fragmentation and spatial distribution of the mineral phase.

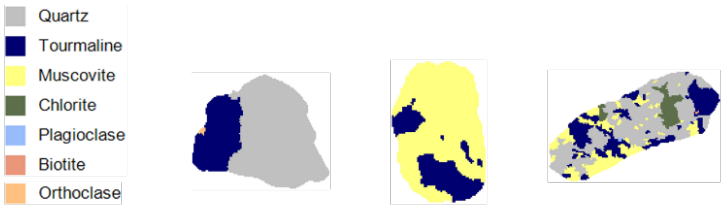

No. of grains	1	6	19
Particle Size (µm)	130.53	139.76	135.51
µ Aspect ratio	0.58	0.57	0.56
µ Circularity	0.56	0.51	0.55
µ Angularity	48.25	71.89	83.47
Form factor	0.75	0.71	0.70
Boundary factor	0.75	0.40	0.18
Surface factor	0.26	0.24	0.24
Texture Index	**0.44**	**0.20**	**0.09**

Figure 6. Effect of grain subdivision on the TI at comparable S_f.

3.5 Grain shape characterization

3.5.1 Circularity, aspect ratio and angularity as a function of grain size

To evaluate the variation in grain morphology across the different size classes, grain shape was characterised using circularity, aspect ratio and angularity. Because no stereological corrections were applied, measurements should be interpreted with caution; nevertheless, consistent general trends in their behaviour were observed across the grain-size classes. Circularity generally decreased from the finest fraction towards the intermediate grain-size classes, with most values ranging from approximately 0.1 to 0.7, which could be classified as slightly to moderately circular. However, this trend was reversed in the +100–250 and +250 µm fractions, where the central circularity values increased. As shown in Fig. 7, the broad overlap between adjacent classes indicates considerable morphological variability, although the coarsest grains tended to exhibit more regular outlines than grains in the intermediate fractions, including a distinct population of very circular grains (~0.7).

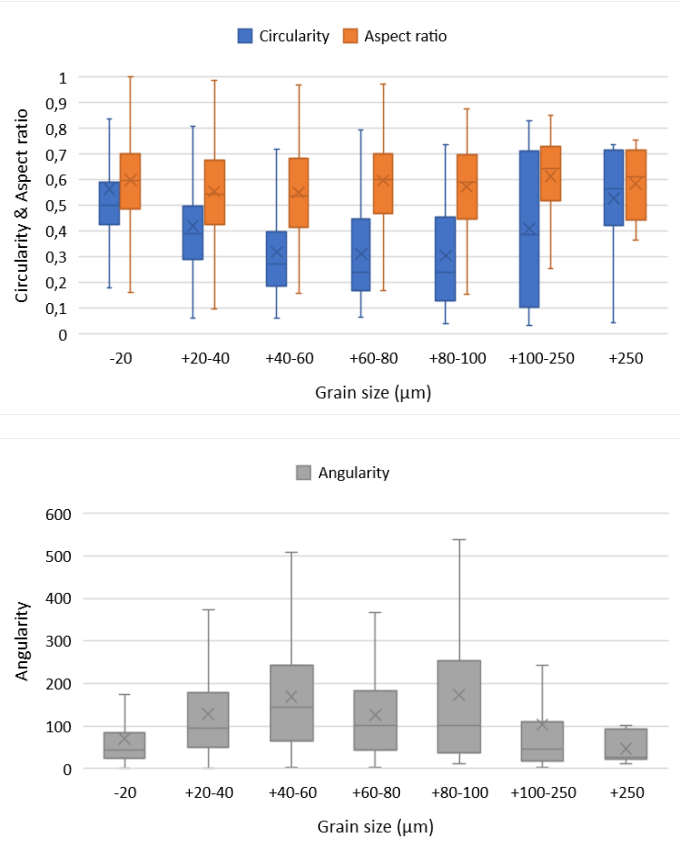

Figure 7. Shape parameters by grain size.

Aspect ratio remained comparatively stable across the complete grain-size range, with most values distributed between approximately 0.4 and 0.7, which could be classified as moderately to slightly elongated. The similarity of the medians and interquartile ranges indicates that grain elongation was largely independent of grain size. Therefore, changes in grain size were not accompanied by a systematic transition from elongated to equant morphologies or vice versa.

Angularity displayed an approximately opposite pattern to circularity. It generally increased from the finest fraction towards the intermediate grain-size classes, indicating progressively more irregular and angular grain boundaries. The largest values and widest distributions occurred mainly between +40–60 and +80–100 µm. Angularity subsequently decreased in the +100–250 and +250 µm fractions, consistent with the simultaneous increase in circularity observed for these coarser grains.

The morphological change in the two coarsest fractions may be related to their higher degree of liberation. When a mineral grain occupies most or all of a particle, its boundary largely coincides with the external particle outline rather than with multiple complex mineral–gangue contacts. The reduction in internal intergrowth boundaries and convoluted mineral interfaces can produce a smoother grain outline, increasing circularity and reducing angularity. Nevertheless, liberation does not necessarily imply rounded grains, because liberated particles may retain angular fracture surfaces generated during comminution. Consequently, the observed increase in circularity and decrease in angularity should be interpreted as being consistent with greater liberation and reduced boundary complexity, rather than as a direct consequence of liberation alone.

3.5.2 Evaluation of grain-shape consistency within particles

To assess the regularity and consistency of grain morphology within individual particles, the mean and median values of circularity and aspect ratio were compared. These parameters were calculated at the particle level, considering particles composed of either a single grain or multiple grains. As shown in Fig. 8, both descriptors exhibit a positive and approximately linear relationship between their mean and median values, indicating that the two measures of central tendency generally provide similar representations of grain shape within each particle. For single-grain particles, the mean and median are necessarily identical and therefore plot directly on the 1:1 line.

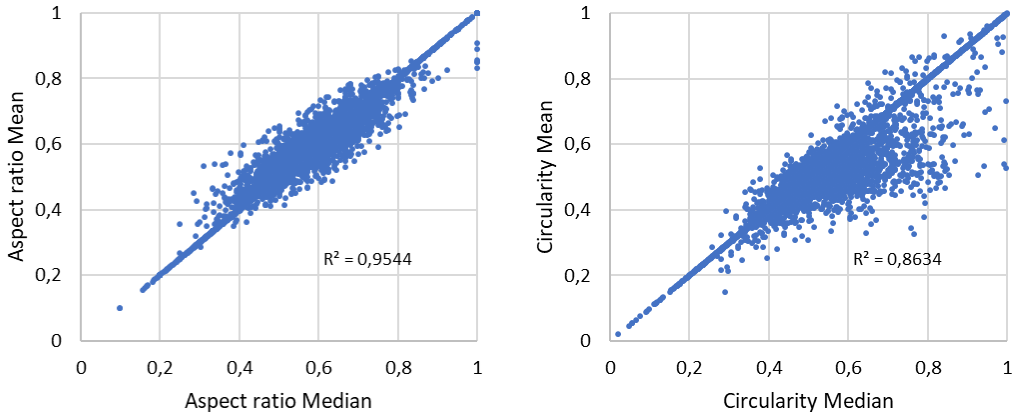

Figure 8. Relationship between mean and median circularity and aspect ratio.

From a statistical perspective, mean and median values that are equal or close indicate that the distribution is centred around a similar representative value and is not strongly asymmetric. For particles containing multiple grains, this agreement suggests that the central morphological value is not substantially affected by grains with exceptionally high or low circularity or aspect ratio. It therefore indicates a general tendency for grain shapes to cluster around the central value. Nevertheless, agreement between the mean and median does not necessarily imply complete morphological uniformity, since a symmetrical distribution may still exhibit considerable dispersion.

The relationship was particularly strong for aspect ratio, with an R^2 of 0.95, meaning that approximately 95% of the variation in the mean aspect ratio is explained by its relationship with the median. This close correspondence indicates relatively consistent grain elongation within individual particles and a limited influence of extreme values. Circularity also showed a strong relationship, with an R^2 of 0.86, although the greater scatter around the 1:1 line indicates higher within-particle variability. This dispersion is more evident at high median circularity values, where the mean frequently deviates towards lower values, suggesting that highly circular grain populations may include some less circular or more irregular grains. Consequently, circularity appears to be more sensitive than aspect ratio to variations in grain-boundary irregularity and to the presence of morphologically contrasting grains within the same particle.

3.6 Relationship between grain shape parameters and the TI

To evaluate how grain morphology contributes to particle texture, the texture index was analysed as a function of aspect ratio, circularity and angularity for different S_f intervals. As shown in Fig. 9, the texture index generally increased with both grain-shape descriptors, although its magnitude was also strongly controlled by the proportion of the target mineral within the particle.

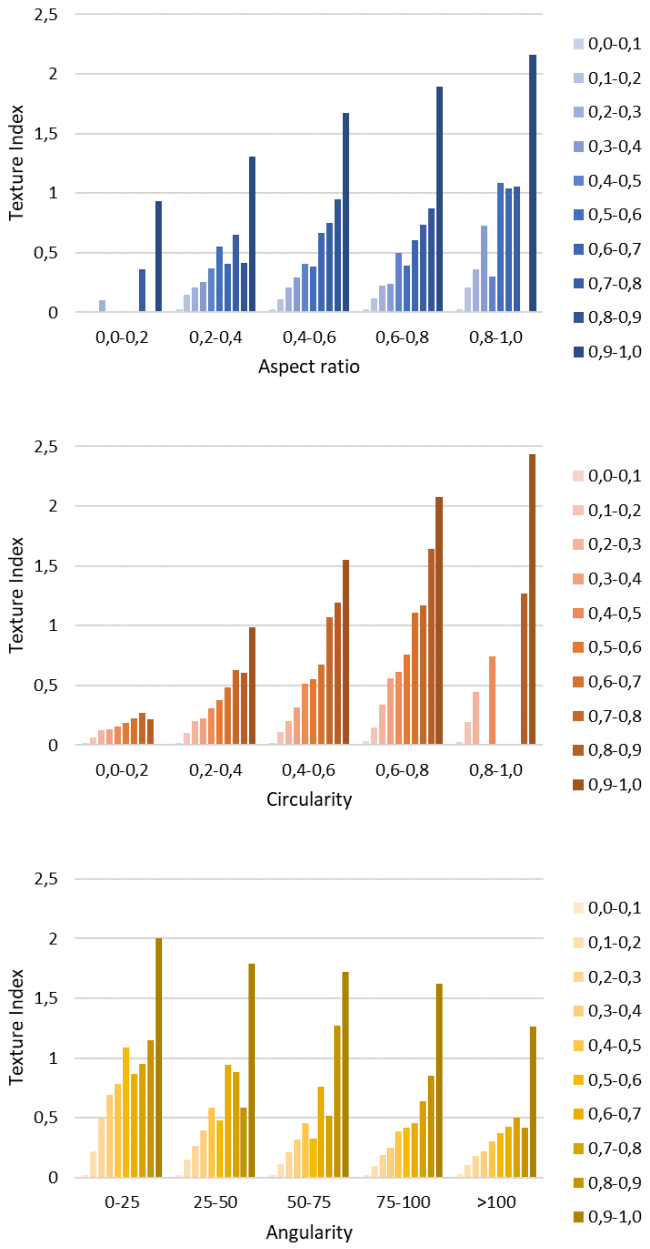

Figure 9. Variation of the TI with shape parameters across S_f intervals.

For aspect ratio, low texture index values were mainly associated with the most elongated grains, represented by aspect ratios below 0.2. The index progressively increased towards the higher aspect-ratio classes, particularly when S_f was also high. Particles with aspect ratios

approaching 1 contained more equant or symmetrical grains and generally attained the highest texture index values. This relationship suggests that particles characterised by compact grain geometries tend to have more favourable textural properties, especially when the target mineral occupies a large proportion of the particle area.

A comparable but more clearly defined trend was observed for circularity. The texture index increased progressively from grains with low circularity to those with more circular outlines. The highest values occurred in particles combining high circularity with high S_f, whereas particles containing irregular grains and a low mineral proportion consistently exhibited low texture index values. Thus, particles with high texture indices are typically characterised by more circular grains and a greater proportion of the target mineral.

Angularity exhibited an inverse relationship with TI. The highest index values occurred in the lowest angularity class and gradually decreased as grains became more angular. Within each angularity interval, TI increased with S_f, indicating that particles combining low angularity with a high mineral proportion achieved the highest values. Conversely, low-TI particles generally contained more angular grains and lower S_f values. This trend reflects the greater boundary irregularity and relative perimeter of angular grains, which reduces F_f and consequently TI.

Together, these trends show that TI increases with grain-shape regularity, represented by higher aspect ratio and circularity and lower angularity, while S_f largely controls the magnitude of the index within each morphological class. The positive relationship with circularity and the negative relationship with angularity are consistent with the formulation of F_f, which compares the area–perimeter relationship of each grain with that of a circle. More circular and less angular grains therefore produce higher F_f values and contribute to a higher TI. Consequently, the highest TI values are associated with high-grade particles containing compact, equant and regular mineral grains.

The particle examples in Fig. 10 further illustrate the influence of grain morphology on the texture index. The three particles have comparable sizes, contain a single tourmaline grain and exhibit similar S_f values, thereby reducing the influence of particle size, grain number and mineral proportion. Under these comparable conditions, differences in TI can be primarily attributed to variations in circularity, aspect ratio and angularity. A more compact grain, characterised by higher circularity, a higher aspect ratio and lower angularity, produces higher F_f and B_f values and therefore a higher TI. Conversely, elongated grains with lower aspect ratios or grains with irregular and angular boundaries exhibit lower circularity and higher angularity, increasing their perimeter relative to their area and consequently reducing the TI.

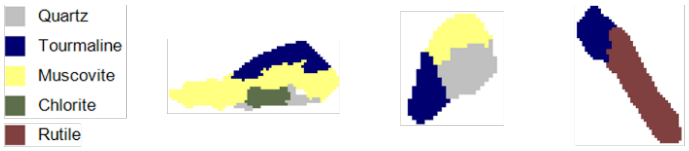

No. of grains	1	1	1
Particle Size (μm)	51.64	41.06	44.23
Aspect ratio	0.34	0.57	0.75
Circularity	0.33	0.54	0.63
Angularity	193.74	54.42	17.36
Form factor	0.57	0.74	0.79
Boundary factor	0.57	0.74	0.79
Surface factor	0.26	0.30	0.28
Texture Index	**0.26**	**0.49**	**0.54**

Figure 10. Effect of grain shape on the TI at comparable S_f.

3.7 Integrated correlation of textural factors and shape parameters

The relationships among grain-shape parameters and textural factors were evaluated using the Pearson correlation (r) matrix presented in Fig.11. The strongest associations were observed among variables describing grain geometry and boundary complexity. Aspect ratio showed a marked negative correlation with angularity, r = −0.61, indicating that more equant or symmetrical grains tend to exhibit less angular and less irregular outlines, whereas elongated grains are generally more angular. This reduction in boundary irregularity may also be associated with a lower perimeter relative to grain area. Aspect ratio was weakly to moderately correlated with F_f, r = 0.29, suggesting that more equant grains tend to be geometrically closer to a circular shape, although aspect ratio and F_f describe different and complementary aspects of grain morphology.

	Aspect ratio	Circularity	Angularity	Form factor	Boundary factor	Surface factor
Aspect ratio	1					
Circularity	0.19	1				
Angularity	-0.61	-0.19	1			
Form factor	0.29	0.82	-0.32	1		
Boundary factor	0.18	0.45	-0.18	0.61	1	
Surface factor	-0.06	-0.07	0.07	-0.09	0.04	1

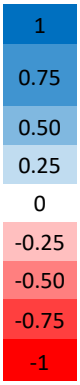

Figure 11. Pearson correlation matrix of textural factors and grain-shape parameters.

Circularity exhibited the strongest correlation in the matrix, showing a strong positive association with F_f, r = 0.82. Thus, grains with higher circularity generally present higher F_f values. This relationship is expected because F_f evaluates the area–perimeter relationship of each grain relative to that of a circle; consequently, a more circular grain has a shorter perimeter for a given area and produces a higher F_f. Circularity was also moderately correlated with B_f, r = 0.45, indicating that more circular grains tend to be associated with lower cumulative perimeter

relative to the total mineral area and, therefore, with more compact mineral domains. Conversely, angularity showed a negative correlation with F_f, $r = -0.32$, confirming that increasingly angular and irregular grains are less similar to a circular geometry and consequently attain lower F_f values.

F_f and B_f were positively correlated, $r = 0.61$, indicating that particles containing grains with regular shapes also tend to exhibit lower overall boundary complexity. This relationship may reflect a tendency for the target mineral to occur as fewer, larger or less fragmented grains, thereby reducing the cumulative perimeter relative to its area. The connection between both factors is particularly clear for particles containing only one mineral grain, for which F_f and B_f have the same value because both are calculated from the area and perimeter of that single grain. In particles containing multiple grains, however, B_f additionally accounts for the cumulative perimeter of the complete grain population and therefore decreases as the mineral becomes more subdivided.

In contrast, S_f displayed negligible correlations with all grain-shape parameters and textural factors, with $|r| \leq 0.09$. This indicates that the proportion of the target mineral within a particle is largely independent of grain circularity, elongation, angularity and boundary regularity. S_f therefore contributes complementary compositional information related to particle grade and mineral abundance, whereas F_f and B_f mainly describe morphological regularity and boundary complexity. All Pearson correlations were statistically significant because of the large number of paired observations, $n = 7{,}961$ and $p < 0.001$. Nevertheless, the very weak correlations involving S_f have limited practical relevance, despite being statistically significant.

4 Conclusions

A particle-based textural index was developed from MLA measurements to integrate three complementary textural attributes: individual grain-shape regularity through F_f, the collective boundary complexity and spatial distribution of the grains through B_f, and the proportion of the target mineral within the particle through S_f. Its multiplicative formulation requires these conditions to be favourable simultaneously, preventing a high value in one factor from compensating for an unfavourable value in another. The index therefore provides information on both grain morphology and particle-scale mineral occurrence that is not fully represented by conventional shape descriptors alone.

S_f exerted the strongest control on TI. The index increased markedly with mineral proportion and reached its highest values in high-grade particles approaching monomineralic composition. TI also decreased as the number of grains per particle increased because mineral subdivision raises the cumulative perimeter and generally reduces B_f and S_f. Consequently, high TI values were primarily associated with particles containing few, compact mineral grains and a high degree of liberation, whereas finely disseminated and compositionally complex particles produced lower values.

Grain morphology provided an additional control on TI. Higher aspect ratio and circularity, together with lower angularity, were consistently associated with higher index values, particularly in particles with high S_f. The close relationship between circularity and F_f confirms that F_f responds directly to increasingly circular and regular grain outlines, while the association between F_f and B_f indicates that morphologically regular grains also tend to occur in more compact arrangements with lower boundary complexity. In contrast, the weak relationships

between S_f and the morphological parameters show that mineral proportion contributes largely independent compositional information, complementing the grain-shape and boundary characteristics represented by F_f and B_f.

These results demonstrate that TI is a sensitive and interpretable metric for distinguishing particles according to mineral proportion, grain subdivision and morphological regularity. MLA provides detailed and consistent quantitative measurements of particle and grain geometry; however, these may be affected by stereological bias. Future studies should therefore apply stereological corrections or complementary 3D characterization methods to better represent true spatial texture and liberation. The present application is also limited to tourmaline in a single material and adopts a binary mineral–gangue representation. Further validation using other minerals, ore types and processing responses is required to establish the broader applicability of the index in mineral-liberation and process-mineralogy studies.

References

Andrews, J., Mika, T., 1975. Comminution of a heterogeneous material: Development of a model for liberation phenomena. Proc. of the 11th Int. Mineral Processing Congress, Cagliari, Italy, 59-88.

Ardalanzdeh, A., Mohammadi, S.D., Sarfarazi, V., Shahbazi, H., 2026. The effects of mineral size, texture coefficient (TC), and ductility–brittleness on creating hole in granitic rock specimens. J. Min. Environ. 17, 295–308. https://doi.org/10.22044/jme.2024.15230.2913.

Atici, U., Comakli, R., 2019. Evaluation of the physico-mechanical properties of plutonic rocks based on texture coefficient. J. South. Afr. Inst. Min. Metall. 119, 63–69. https://doi.org/10.17159/2411-9717/2019/v119n1a8.

Ersoy, A., Waller, M.D., 1995. Textural characterisation of rocks. Eng. Geol. 39, 123–136. https://doi.org/10.1016/0013-7952(95)00005-Z.

Escalante, P., Oliva, J., Anticoi, H., Hoffmann Sampaio, C., Mohanty, K., 2025. Characterization of mineralogical impurities in a carbonate-rich material using MLA. Miner. Eng. 230, 109409. https://doi.org/10.1016/j.mineng.2025.109409.

Escalante, P., Oliva, J., Anticoi, H., Hoffmann Sampaio, C., Ochoa, G., Cortina, J.L., 2026. MLA-based characterization of fine iron sulfide particles and implications for critical metal recoveries. Powder Technol. 474, 122301. https://doi.org/10.1016/j.powtec.2026.122301.

Fandrich, R., Gu, Y., Burrows, D., Moeller, K., 2007. Modern SEM-based mineral liberation analysis. Int. J. Miner. Process. 84, 310–320. https://doi.org/10.1016/j. minpro.2006.07.018.

Ferrara, G., Preti, U. and Meloy, T.P., 1989. Inclusion shape, mineral texture and liberation. Int. J. Miner. Process., 27: 295-308. https://doi.org/10.1016/0301-7516(89)90070-7.

Gu, Y., 2003. Automated scanning electron microscope based mineral liberation analysis: An introduction to JKMRC/FEI Mineral Liberation Analyser. J. Miner. Mater. Charact. Eng. 2 (1), 33–41. https://doi.org/10.4236/jmmce.2003.21003.

Hilden, M., Powell, M., 2017. A geometrical texture model for multi-mineral liberation prediction. Miner. Eng. 111, 25–35. https://doi.org/10.1016/j.mineng.2017.04.020.

Kamani, M., Ajalloeian, R., 2019. Evaluation of engineering properties of some carbonate rocks trough corrected texture coefficient. Geotech. Geol. Eng. 37, 599–614. https://doi.org/10.1007/s10706-018-0630-8.

Karakaya, E., Kekeç, B., Bilim, N., Adigözel, F.V., 2025. A new approach for calculating texture coefficients of different rocks with image segmentation and image processing techniques. Microsc. Res. Tech. 88, 2612–2629. https://doi.org/10.1002/jemt.24879.

King, R.P., 2001. Mineral liberation, in: Modeling and Simulation of Mineral Processing Systems. Butterworth-Heinemann, Oxford. https://doi.org/10.1016/B978-0-08-051184-9.50007-9.

Lee, D., Je, J., Kim, K., Kwon, J., Cho, H., 2022. Prediction of iron ore mineral liberation behavior using the Andrews–Mika diagram and beta distribution. Adv. Powder Technol. 33, 103558. https://doi.org/10.1016/j.apt.2022.103558.

Leißner, T., Bachmann, K., Gutzmer, J., Peuker, U.A., 2016. MLA-based partition curves for magnetic separation. Miner. Eng. 94, 94–103. https://doi.org/10.1016/j.mineng.2016.05.015.

Månbro, C., Parian, M., Rosenkranz, J., 2025. Exploring the role of ore texture in comminution and approaches to identify and promote non-random breakage. Miner. Eng. 230, 109405. https://doi.org/10.1016/j.mineng.2025.109405.

Mata, J., 2012. Recorregut de recerca de geològica per les terres de la ribera de l'Ondara, a través del Pla d'Urgell, de l'Urgell i de la Segarra: des de Bellpuig d'Urgell a Ivars d'Urgell, Barbens, Tàrrega, Cervera, La Panadella i a Guimerà. Xaragall: Revista de Ciències de La Catalunya Central, 448, 1–16. https://hdl.handle.net/2099/12455.

Mikaeil, R., Bakhtavar, E., Hosseini, S., Jafarpour, A., 2022. Fuzzy classification of rock engineering indices using rock texture characteristics. Bull. Eng. Geol. Environ. 81, 312. https://doi.org/10.1007/s10064-022-02807-8.

Ozturk, C.A., Nasuf, E., 2013. Strength classification of rock material based on textural properties. Tunn. Undergr. Space Technol. 37, 45–54. https://doi.org/10.1016/j.tust.2013.03.005.

Ozturk, C.A., Nasuf, E., Kahraman, S., 2014. Estimation of rock strength from quantitative assessment of rock texture. J. South. Afr. Inst. Min. Metall. 114, 471–480. https://scielo.org.za/scielo.php?script=sci_arttext&pid=S2225-62532014000600013.

Pérez-Barnuevo, L., Pirard, E., Castroviejo, R., 2012. Textural descriptors for multiphasic ore particles. Image Anal. Stereol. 31, 175–184. https://doi.org/10.5566/ias.v31.p175-184.

Pérez-Barnuevo, L., Pirard, E., Castroviejo, R., 2013. Automated characterisation of intergrowth textures in mineral particles. A case study. Miner. Eng. 52, 136–142. https://doi.org/10.1016/j.mineng.2013.05.001.

Ueda, T., Oki, T., Koyanaka, S., 2017. Comparison of seven texture analysis indices for their applicability to stereological correction of mineral liberation assessment in binary particle systems. Minerals. 7, 222. https://doi.org/10.3390/min7110222.

Voigt, M.J., Miller, J., Bbosa, L., Govender, R.A., Bradshaw, D., Mainza, A., Becker, M., 2019. Developing a 3D mineral texture quantification method of drill core for geometallurgy. J. South. Afr. Inst. Min. Metall. 119, 347–353. http://dx.doi.org/10.17159/2411-9717/590/2019.

Zhang, J., Subasinghe, N., 2013. Prediction of mineral liberation characteristics of comminuted particles of high-grade ores. Miner. Eng. 49, 68–76. https://doi.org/10.1016/j.mineng.2013.05.005.